FLOW ABOUT A CYLINDER IN A NARROW GAP AT HIGH VELOCITIES

V. D. Zhak, V. E. Nakoryakov, and S. A. Safonov

UDC 532.546

The Hele–Shaw cell is widely used to model filtration processes at low velocities [1]. Filtration at high velocities has not been adequately studied. Measurements were presented in [2, 3] of the velocity and friction profiles on the wall and spectral characteristics of propagation of a jet in a thin slit, and a model was proposed for a laminar stream. Real porous plates contain structural formations, including impermeable formations. This makes it necessary to study flow about a body of arbitrary form in a thin slit. The approach proposed in [4] demonstrated that the inertial terms of the equations of motion must be considered even at Re > 10 ($Re = 2u_0h/\nu$, u_0 is the mean mass rate of the flow, h is the thickness of the slit).

Here we propose to solve a steady problem concerning flow of an incompressible fluid about a cylinder in a Hele–Shaw cell. We will take into account convective terms of the equations of motion and compare Doppler-laser measurements of velocity of flow about the cylinder with the results of a numerical calculation.

Steady flow of an incompressible fluid about a circular cylinder in Hele–Shaw cells is described in the general case by the equation

$$V\nabla V = -\frac{1}{\rho}\nabla p + \nu\Delta V, \quad \nabla V = 0. \tag{1}$$

Adhesion conditions are satisfied on the plane surface of the slit (z = 0 and z = h) and on the lateral surface of the cylinder, the generatrices of which are perpendicular to the surfaces of the slit. The flow is assumed to be uniform and undisturbed at infinity.

We will assume that in a narrow slit, i.e., when $h \ll r_0$ (r_0 is the radius of the cylinder), there is no motion in the z direction even near the lateral walls of the cylinder (w = 0), while the Poiseuille profile is realized for the longitudinal u and transverse v components of velocity

$$u(x, y, z) = 4u_+(x, y)\frac{z}{h}\left(1 - \frac{z}{h}\right), \quad v(x, y, z) = 4v_+(x, y)\frac{z}{h}\left(1 - \frac{z}{h}\right). \tag{2}$$

After integration over z from 0 to h, we obtain initial system (1) in the form

$$u_+\frac{\partial u_+}{\partial x} + v_+\frac{\partial u_+}{\partial y} = -\frac{15}{8\rho}\frac{\partial p}{\partial x} + \frac{5}{4}\nu\left(\frac{\partial^2 u_+}{\partial x^2} + \frac{\partial^2 u_+}{\partial y^2} - \frac{12}{h^2}u_+\right), \tag{3}$$

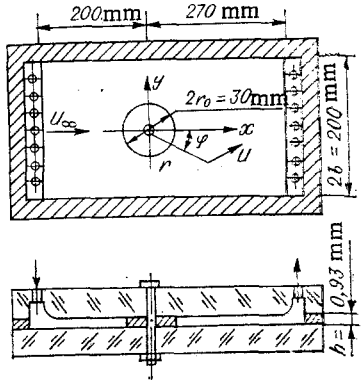

Fig. 1

Novosibirsk. Translated from Zhurnal Prikladnoi Mekhaniki i Tekhnicheskoi Fiziki, No. 2, pp. 30-34, March-April, 1986. Original article submitted February 12, 1985.

0021-8944/86/2702-0180$12.50

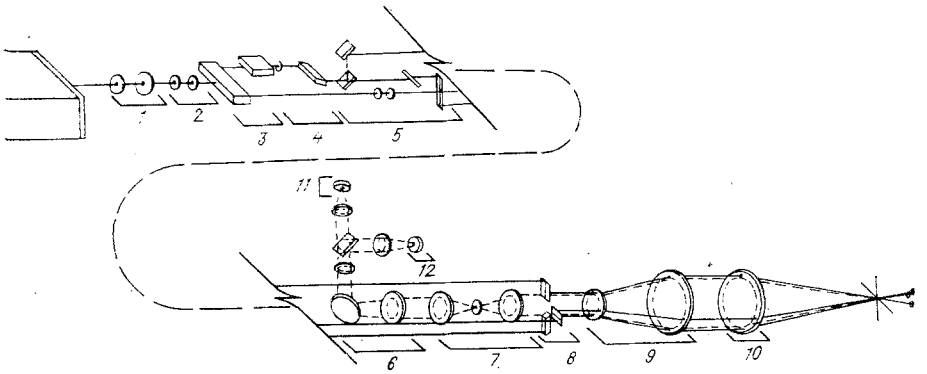

Fig. 2

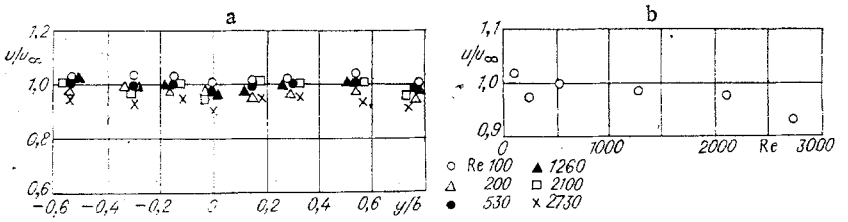

Fig. 3

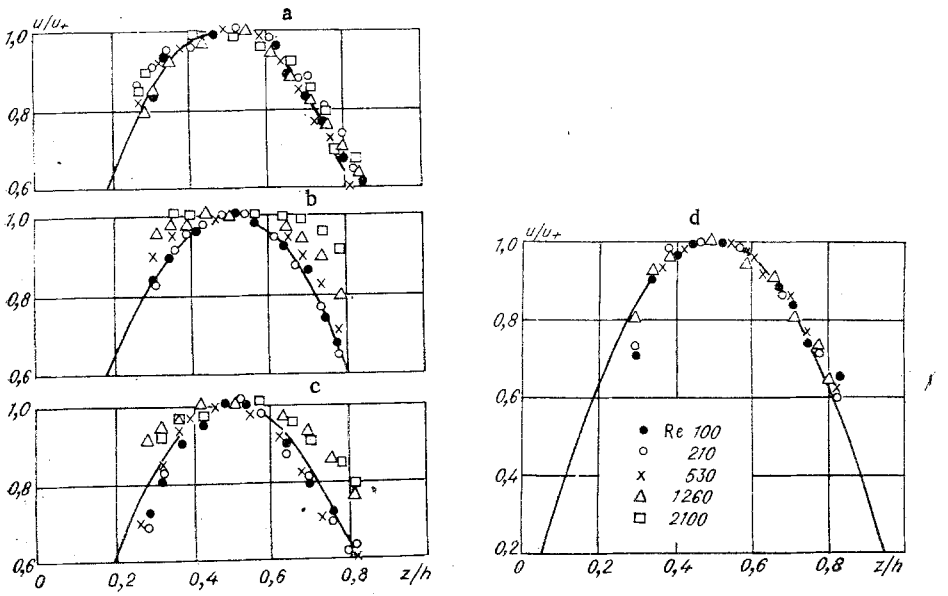

Fig. 4

$$u_+\frac{\partial v_+}{\partial x}+v_+\frac{\partial v_+}{\partial y}=-\frac{15}{8\rho}\frac{\partial p}{\partial y}+\frac{5}{4}\nu\left(\frac{\partial^2 v_+}{\partial x^2}+\frac{\partial^2 v_+}{\partial y^2}-\frac{12}{h^2}v_+\right),\quad \frac{\partial u_+}{\partial x}+\frac{\partial v_+}{\partial y}=0. \tag{3}$$

Having written Eq. (3) in dimensionless variables ψ–ω (the stream function versus vorticity) and polar coordinates r and φ, we have

$$\frac{\partial}{\partial r}\left(\omega\frac{\partial\psi}{\partial\varphi}\right)-\frac{\partial}{\partial\varphi}\left(\omega\frac{\partial\psi}{\partial r}\right)=\frac{5}{3\,\mathrm{Re}}\left\{\left[\frac{\partial}{\partial r}\left(r\frac{\partial\omega}{\partial r}\right)+\frac{1}{r}\frac{\partial^2\omega}{\partial\varphi^2}\right]\frac{h}{r_0}-12\frac{r_0}{h}r\omega\right\},$$

$$\frac{\partial}{\partial r}\left(r\frac{\partial\psi}{\partial r}\right)+\frac{1}{r}\frac{\partial^2\psi}{\partial\varphi^2}=r\omega,$$

where $\psi=\psi_+/(1.5u_0r_0)$; $\omega=\omega_+r_0/(1.5u_0)$; ψ_+ and ω_+ are the dimensional stream function and vorticity.

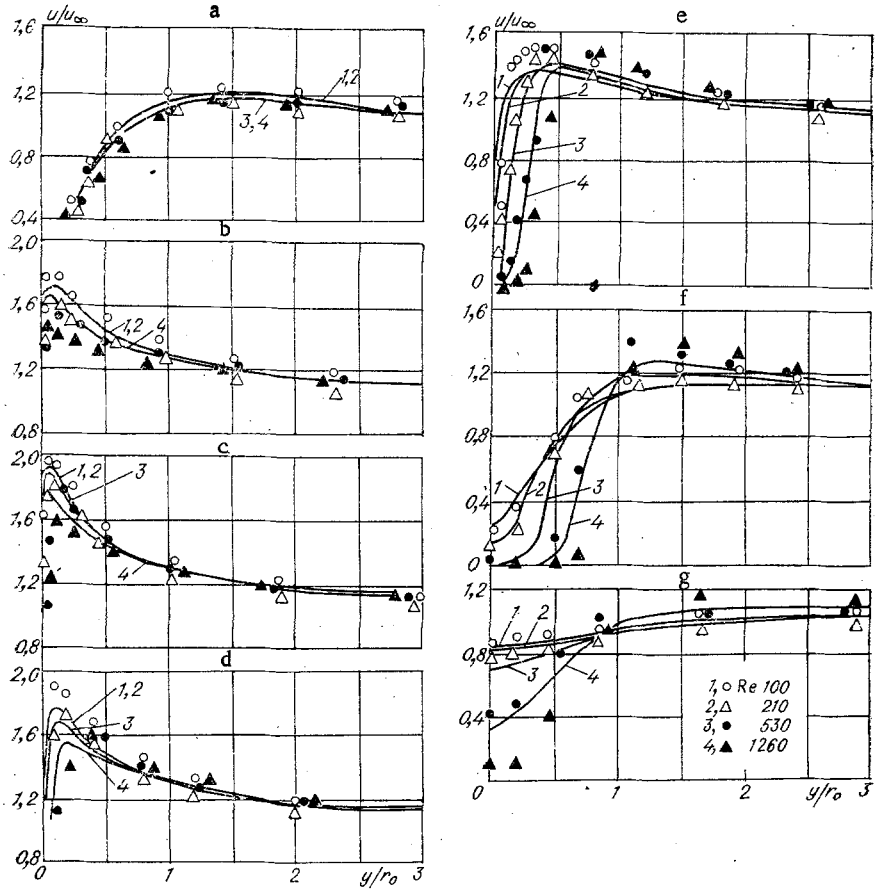

Fig. 5

System (4) was integrated numerically on a nonuniform 33 × 61 grid, and we used the conditions of adhesion on the cylinder wall in Buds' form [5]

$$\omega_p = -0.5\omega_s + \frac{3}{r_{ps}^2}(\psi_s - \psi_p),$$

where p pertains to values of the variables ψ and ω at the grid node on the wall. The subscript s pertains to values of the variables at the next node along the normal from the wall, while r_{ps} represents the distance between the nodes p and s. The convective terms were approximated by directional one-sided differences, the terms with second derivatives were approximated by central differences, and the source terms were approximated by the arithmetic mean at the nodes of the control volume.

Comparison of the calculations on 33 × 61 and 17 × 31 grids shows that the numerical solution is sufficiently invariant to the dimensions of the grid for Re ≤ 200 (the difference in the velocity values is about 5%).

The fields of flow velocity about a cylinder in a narrow gap were measured on a unit with a tank filled to a constant level. A drop in height between the upper and lower tanks was ensured by having the fluid move at a maximum Reynolds number Re = 2730. Figure 1 shows the design of the working section. A 30-mm-diameter cylinder with a thickness h = 0.93 mm (slit thickness) was placed 200 mm from the 16 × 12 mm inlet header. The inlet and outlet headers were joined to the wall of the through part of the unit over a radius of 4 mm. The walls of the working section were made of polished organic glass and were 24 mm thick.

The measurements were made with a model 9100-8 Doppler-laser velocity meter made by the TSI company. The total radiation intensity of the model 165-04 laser, made by the "Spectrophysics" company, ranged from 100 to 400 mW at wavelengths of 488 and 514.5 nm. Two orthogonal interference grids were formed with blue and green light in the measurement volume, which was 30 μm in diameter and 180 μm long.

The optical system of the velocity meter is shown in Fig. 2. The transmitting component consists of a collimator 1, phase plates 2, splitter 3, shift cell 4, dichoric color-separation scanner 5, beam-broadening blocks 8 and 9, and a focusing lens 10 with a focal length of 120 mm. The receiving component includes a focusing lens and a field stop 7, tilting mirrors 6 with interference filters for wavelengths of 488 and 514.5 nm, and photomultipliers 11 and 12 with field stops at the inlet.

The signal was analyzed by a model 1980 computing processor made by the TSI company and was then analyzed on a computer. A total of 4000 samples separated by a time interval of 0.006-0.025 sec were analyzed at each measurement point. The location of the measurement volume of the velocity meter in the plane of the model was fixed by a coordinate spacer to within 0.05 mm, while the z coordinate was measured with a dial gauge with 0.01-mm graduations.

The measured velocity distribution over the width of the slit 2b on the axis of the gap ($z/h = 0.5$) in front of the cylinder (in the section $x/r_0 = -5.8$) is shown in Fig. 3a. The velocity is dimensionless in regard to $u_\infty = 1.5u_0$. Figure 3b shows the dependence of the mean velocity across the slit on Re on the axis of the gap (in the same section). It is evident that flow in the slit is uniform widthwise away from the cylinder, while the velocity on the axis of the gap corresponds to the relation for profile (2) ($u = 1.5u_0$) up to Re = 2100, inclusively.

Figure 4a-d shows direct measurements of the profile of the tangential velocity component over the thickness of the slit near the cylinder (u_+ is the maximum velocity in the given section). Figure 4a, b shows velocity profiles over the slit thickness in front of the cylinder at the points with the coordinates $(r - r_0)/h = 18.1$, $\varphi = -135°$ and $(r - r_0)/h = 1.36$, $\varphi = -135°$. Figure 4c, d corresponds to points behind the cylinder with the coordinates $(r - r_0)/h = 6.68$, $\varphi = 45°$, and $(r - r_0)/h = 3.64$, $\varphi = 45°$. The line shows the Poiseuille profile. The measurements in Fig. 4 illustrate that the parabolic velocity profile over the slit thickness is deformed near the cylinder wall at large Re (the profile becomes fuller). In the range Re = 100-1260, the parabolic approximation agrees satisfactorily with the measured velocity profiles over the slit thickness in front of and behind the cylinder.

Figure 5a-g compares measured profiles of total velocity on the gap axis for several sections x/r_0 in the coordinates u/u_∞ and y/r_0. The solid lines show results of the numerical calculation; the coordinate y in the sections $x/r_0 = -1$, 1.2, and 2.5 (a, f, g) was reckoned from the symmetry axis of the model (see Fig. 1); in the sections $x/r_0 = -0.5$, 0, 0.4, and 0.8 (b-e), the y coordinate was reckoned from the cylinder wall. The calculations and measurements showed that at Re > 100 the action of inertial forces leads to stratification of the velocity profiles with respect to Re.

Reverse flow was observed in the aft region of the cylinder in tests with Re > 1260. The velocity of these flows in this region was less than $0.06u_0$ (the calculation shows that vortices develop in this region at Re > 300).

On the whole, the calculation agrees with the experiment up to Re = 1260; for Re = 100, 200, and 500, satisfactory quantitative agreement was obtained between the experimental and calculated data. The proposed theoretical model for describing flow about a cylinder in a Hele–Shaw cell makes it possible to account for inertial effects.

LITERATURE CITED

1. Ya. Ber, D. Zaslavski, and S. Irmei, Physicomathematical Principles of Water Filtration [Russian translation], Mir, Moscow (1971).
2. V. D. Zhak, V. A. Mukhin, et al., "Propagation of a submerged jet in a narrow slit," Zh. Prikl. Mekh. Tekh. Fiz., No. 3 (1985).
3. O. N. Kashinskii, B. K. Koz'menko, V. E. Nakoryakov, and I. A. Pavlov, "Experimental study of flow hydrodynamics in the discharge of a liquid into a gap between parallel surfaces," in: Physical Processes in the Development of Geothermal Fields [in Russian], Leningr. Gornyi Inst., Leningrad (1983).
4. F. Riegels, "Zur kritik des Hele-Shaw-Versuchs," Z. Angew. Math. Mech., 18, No. 2 (1938).
5. P. J. Roache, Computational Fluid Dynamics, Hermosa (1976).